polysaccharides

MDPI

Article

Chitosan and Collagen-Based Materials Enriched with Curcumin (*Curcuma longa*): Rheological and Morphological Characterization

Eduardo P. Milan [1], Mirella Romanelli V. Bertolo [2,*], Virginia C. A. Martins [2], Stanislau Bogusz Junior [2] and Ana Maria G. Plepis [1,2]

[1] Interunits Graduate Program in Bioengineering (EESC/FMRP/IQSC), University of Sao Paulo (USP), Sao Carlos 13560-970, Brazil; epmilan@usp.br (E.P.M.); amplepis@iqsc.usp.br (A.M.G.P.)
[2] Sao Carlos Institute of Chemistry, University of Sao Paulo (USP), Sao Carlos 13560-970, Brazil; virginia@iqsc.usp.br (V.C.A.M.); stanislau@iqsc.usp.br (S.B.J.)
* Correspondence: mirella.bertolo@usp.br

Abstract: In this study, chitosan and collagen (Ch: Col)-based materials containing curcumin (Cur) as a bioactive compound were developed for wound-healing purposes. The effects of incorporating curcumin and increasing its concentration on both the rheological properties of the formed solutions and the morphological and thermal properties of the three-dimensional scaffolds obtained from them were evaluated. Rheology showed that the presence of curcumin resulted in solutions with a solid-like behavior (G′ > G″), higher collagen denaturation temperatures, and higher viscosities, favoring their use as biomaterials for wound healing. A greater cross-linking effect was observed at higher curcumin concentrations, possibly between the amino groups from both polymers and the hydroxyl and keto groups from the polyphenol. Such cross-linking was responsible for the delay in the onset of degradation of the scaffolds by 5 °C, as revealed by thermogravimetric analysis. Moreover, the pore diameter distribution profile of the scaffolds changed with increasing curcumin concentration; a greater number of pores with diameters between 40 and 60 µm was observed for the scaffold with the highest curcumin content (50 mg), which would be the most suitable for the proposed application. Thus, the materials developed in this study are presented as promising biomaterials for their biological evaluation in tissue regeneration.

Keywords: chitosan; collagen; curcumin; *Curcuma longa*; scaffolds; rheology

check for updates

Citation: Milan, E.P.; Bertolo, M.R.V.; Martins, V.C.A.; Bogusz Junior, S.; Plepis, A.M.G. Chitosan and Collagen-Based Materials Enriched with Curcumin (*Curcuma longa*): Rheological and Morphological Characterization. *Polysaccharides* **2022**, *3*, 236–249. https://doi.org/10.3390/polysaccharides3010013

Academic Editor: Azizur Rahman

Received: 22 January 2022
Accepted: 15 February 2022
Published: 17 February 2022

Publisher's Note: MDPI stays neutral with regard to jurisdictional claims in published maps and institutional affiliations.

Copyright: © 2022 by the authors. Licensee MDPI, Basel, Switzerland. This article is an open access article distributed under the terms and conditions of the Creative Commons Attribution (CC BY) license (https://creativecommons.org/licenses/by/4.0/).

1. Introduction

Wounds are discontinuities created in healthy tissue that can be caused by chemical, physical, and immunological processes, among others. The wound-healing process comprises several steps, ranging from healing through inflammation to the induction of cell proliferation [1,2]. One of the main factors that can negatively affect the wound-healing process is the attack of free radicals, which are highly unstable species capable of oxidizing the new cells that have been proliferating around the wound, thus damaging them and delaying the healing process [3].

The use of biomaterials stands out as one of the best alternatives for the wound-healing process due to their biocompatibility, non-toxicity, capacity to induce cell interactions and responses, and their capacity for tissue regeneration [4,5]. In this sense, chitosan and collagen are two options of polymers that are extensively used as biomaterials, individually or in combination [6–9]; chitosan, a polysaccharide derived from chitin, has advantages due its antimicrobial activity and its positive charge in solution [10–12]; collagen, the most abundant protein found in bone and tendons, acts as an extracellular matrix in the control of the function, structure, and shape of tissues [13].

One of the ways to improve both the physicochemical and biological properties of chitosan- and collagen-based biomaterials involves the addition of nutraceutical compounds that also act as cross-linkers; curcumin, a yellowish pigment found in turmeric (*Curcuma longa*), is one of these compounds [14]. Its keto and hydroxyl groups can promote the cross-linkage of polymers, thus increasing their structural stability, and its numerous biological properties (such as anti-inflammatory, anti-fungal, anti-cancer, and anti-invasive properties) also improve the performance of the formulated biomaterials [4,15,16]. Moreover, the proven antioxidant activity of curcumin makes its application in preventing oxidation and scavenging free radicals useful in the wound-healing process.

The interaction between curcumin with both chitosan and collagen has already been elucidated in several studies in the literature, many of which propose the use of these biomaterials for application in wound healing. Dharunya et al. (2016) [4] developed an aerogel based on cross-linked collagen with curcumin, which presented controlled anti-proteolytic activity, making it a suitable 3D scaffold for biomedical applications. In another study, Rezaei et al. (2018) [17] developed chitosan and collagen scaffolds containing curcumin nanoparticles; the scaffolds with the best physicochemical properties were those containing the polymers in a 2:1 ratio (chitosan: collagen), with and without curcumin nanoparticles incorporated. However, the scaffolds without the nanoparticles did not cause any up-regulation in TGF-β1 or Smad7 mRNA expression; therefore, they were unable to accelerate the wound-healing process, while the scaffolds containing curcumin were effective in this acceleration [18]. In a recent study, a combination of chitosan, collagen, and curcumin was tested in the form of electrospun nanofibers containing polyethylene oxide, which also targeted the wound-healing process [19]. Curcumin was successfully released from the nanofibers for up to 3 days and did not cause any significant cytotoxicity to human dermal fibroblasts, which also makes its use and incorporation in other types of biomaterials, such as three-dimensional scaffolds, promising.

As far as we know, the aforementioned studies with the combination of chitosan, collagen, and curcumin did not conduct any rheological characterizations of these materials, which, once well detailed (with oscillation, temperature, and flow tests, for example), can be combined with the thermal, morphological, and structural properties observed for the scaffolds. Moreover, rheology can unravel how the incorporation of curcumin may affect the stability of the polymeric matrix against deformation, shear, and temperature at the molecular level. Thus, the aim of this study was to develop chitosan- and collagen-based materials with different concentrations of curcumin and to analyze their rheological profiles (viscoelastic and steady shear), as well as the structural and thermal characteristics of the scaffolds formed. The materials developed were suitable for the proposed application with their solid-like behavior, high collagen denaturation temperatures, and high viscosities.

2. Materials and Methods

2.1. Materials

All solvents and reagents were of analytical grade and were used as such. The squid pens used as a source of β-chitin for chitosan preparation were obtained at Miami Comércio e Exportação de Pescados Ltda (Cananéa, SP, Brazil). The bovine tendon used for collagen extraction was obtained at Casa de Carnes Santa Paula(São Carlos, SP, Brazil). Curcumin was purchased from a local manipulation drugstore (São Carlos, SP, Brazil).

2.2. Methods

2.2.1. Chitosan Obtention

Chitosan was obtained from squid pens (*Doryteuthis* spp.) through a demineralization, deproteinization, and deacetylation process adapted from Horn, Martins, Plepis (2009) [20]. Briefly, the procedure involved the removal of impurities with a 0.55 mol L^{-1} HCl solution, followed by the extraction of β-chitin in an alkaline medium (0.3 mol L^{-1} NaOH, 1 h, 80 °C); finally, a new alkaline treatment (NaOH 40% *w/w*, 80 °C, 3 h, N_2 flow) led to the deacetylation of β-chitin and obtention of chitosan, which was washed to neutrality and

dried. The reaction yield was 26.44%, and the chitosan acetylation degree and molecular weight were 5.68 ± 0.05% and 205 kDa, respectively, as determined according to the procedures developed by Lavertu et al. (2003) [21] and Rinaudo (2006) [22].

2.2.2. Collagen Obtention

The extraction of collagen from the bovine tendon followed the procedure described by Horn, Martins, and Plepis (2009) [20] and started with the removal of unwanted organic materials by washing in a 0.9% (*w/w*) saline solution (NaCl) and in deionized water until completely clean. Then, the tendon was submitted to hydrolysis in an alkaline solution (pH > 12) containing chlorides and sulfates of Na^+, K^+, and Ca^{2+} for 96 h. After this period, the tendon was removed from alkaline conditions and placed in another solution containing sulfates and chlorides of Na^+, K^+, and Ca^{2+} ions for 6 h. The excess salts were removed by washing in a 3% (*w/w*) boric acid solution and deionized water (3 h each), followed by washing in a 0.3% (*w/w*) EDTA solution and deionized water (3 h each). Finally, type I collagen was extracted and maintained in a pH 3.5 acetic acid (HAc) solution. Its concentration of 1% (*w/w*) was determined by weighing after lyophilization in a Freeze Dryer Modulyo model (Edwards High Vacuum International, West Sussex, UK).

2.2.3. Curcumin Purification

The purification process of commercial curcumin was carried out by dissolving the powder in a 1% HAc/ethanol solution (20:1 ratio) at room temperature and under protection from light until complete solubilization. The solution was then filtered, the ethanol was removed by evaporation for 24 h, and the purified curcumin solution was lyophilized for 16 h to obtain a thin powder.

2.2.4. Preparation of Chitosan/Collagen/Curcumin Scaffolds

To prepare the solutions containing chitosan, collagen, and curcumin, both polymers were solubilized separately in 1% (*w/w*) HAc at a concentration of 1% (*w/w*), leading to the Ch and Col solutions. These solutions were mixed in a 1:1 ratio at room temperature, leading to Ch: Col (without curcumin) solution. Next, curcumin (Cur) was dissolved in 1 mL of HAc 1% at concentrations of 10, 20, and 50 mg; 1 mL of Cur solution was mixed with 20 g of the polymeric solutions, resulting in the Ch: Col: Cur10, Ch: Col: Cur20, and Ch: Col: Cur50 solutions. For the preparation of scaffolds, the air was removed from the solutions, which were placed in Teflon® molds, frozen, and lyophilized.

2.2.5. Fourier Transform Infrared Spectroscopy (FTIR)

FTIR analysis was conducted to identify the main functional groups of chitosan, collagen, and curcumin, as well as to verify the interactions between them in the Ch: Col: Cur20 sample. For that, chitosan and curcumin (previously dried) were mixed in $KBr_{(s)}$; collagen, in turn, was diluted in HAc with a pH 3.5 (final concentration of 0.2%), placed in Teflon® molds, and dried under air flow to form a film through the casting method. The equipment used was an FTIR Shimadzu IR Affinity–1 (Shimadzu, Kyoto, Japan), and the spectra were obtained in the region of 4000–400 cm^{-1} with 32 scans and a resolution of 4 cm^{-1}.

2.2.6. Rheological Assays

The rheological study was performed with the Ch: Col, Ch: Col: Cur10, Ch: Col: Cur20, and Ch: Col: Cur50 solutions in an AR-1000 N stress-controlled rheometer (TA Instruments, New Castle, DE, USA) with a cone/stainless steel plate geometry of 60 mm in diameter, angle of 0° 30′, and a fixed gap of 15 μm. The temperature was controlled with a Peltier system. Prior to measurements, the prepared solutions were stored under refrigeration and protected from light. The rheological assays started with the determination of the linear viscoelastic region (LVR) of the solutions in the strain sweep measurements, from 0.01 to 100 Pa, at a frequency of 1.0 Hz and at 25 °C; then, the behavior of the viscous (G″) and

elastic (G′) moduli of the solutions were evaluated as a function of temperature from 25 to 75 °C with a heating ratio of 5 °C min^{-1} at a fixed strain and frequency of 10% and 1 Hz, respectively. Finally, flow tests determined the viscosity of the solutions while varying the shear rate from 1 to 1000 s^{-1} at 25 °C.

2.2.7. Thermogravimetric Analysis (TGA)

The thermogravimetric profile of the chitosan/collagen/curcumin scaffolds was assessed with TGA-Q50 equipment (TA Instruments, New Castle, DE, USA). A sample of 5–6 mg was used, with a temperature range from 25 to 800 °C at 10 °C min^{-1} under a synthetic air atmosphere (60 mL min^{-1}).

2.2.8. Scanning Electron Microscopy (SEM)

The morphology of the scaffolds—both the surface and cross-sectional surface—was observed using a ZEISS LEO 440 instrument (Zeiss, Cambridge, UK) with an OXFORD detector (model 7060) and an electron beam of 20 kV. Before the analysis, the scaffolds were covered with a 6 nm gold layer. The diameters of the scaffolds pores and channels were calculated using the UTHSCSA Image Tool software. For each scaffold, 20 measurements were performed in the surface and cross-sectional surface photomicrographs at 500× and 1000× magnification, respectively.

2.2.9. Statistical Analysis

The Shapiro–Wilk test was used to verify the data distribution. The results for the pore and channel size were examined using analysis of variance (ANOVA), followed by Tukey's test, with a significance level of 5%.

3. Results and Discussion

3.1. Fourier Transform Infrared Spectroscopy (FTIR)

The FTIR spectra of chitosan, collagen, curcumin, and the Ch: Col: Cur20 scaffold are shown in Figure 1. The spectra allow the identification of bands referring to the main functional groups of both polymers and curcumin; this was also a structural identification of this compound, which was of commercial origin. In Figure 1a, the characteristic bands of chitosan are observed, with an emphasis on the broad band in the region of 3700–3100 cm^{-1}, which is related to the axial deformations of the O-H and N-H bonds present in the polysaccharide structure (Table 1). Such deformations are also responsible for the band of lower intensity observed in the region of 3300 cm^{-1} for collagen in the spectrum in Figure 1b. Regarding curcumin, the main bonds that lead to the broad band observed between 3360 and 3450 cm^{-1} are the O-H bonds of the phenolic rings present in the curcuminoid structure (Figure 1c).

Other characteristic bands can be observed along the spectra, such as those present in the region of 1660–1653 cm^{-1}; in the case of the polymers, these bands arise due to the stretching of the C=O bonds of the carbonyls that comprise amide I [23,24]. In relation to curcumin, the band at 1660 cm^{-1} refers to the C=O bonds of the beta-diketone found in the central region of the molecule, which can lead to an intermolecular hydrogen atom transfer and to a keto-enol tautomerism [25].

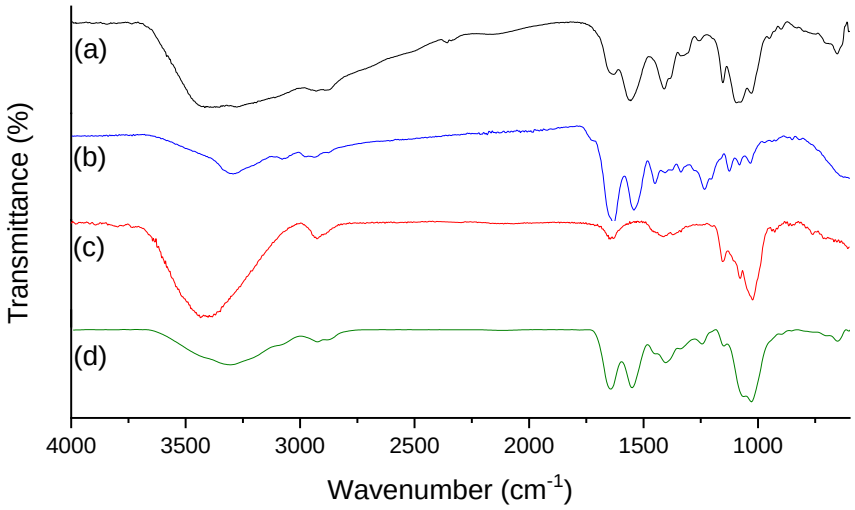


Figure 1. FTIR spectra of chitosan (**a**), collagen (**b**), curcumin (**c**), and Ch: Col: Cur20 scaffold (**d**).

Table 1. Characteristic FTIR bands of chitosan, collagen, and curcumin.

Wavenumber (cm^{-1})	Chitosan	Collagen	Curcumin
3700–3100	O-H and N-H deformation		
3300		O-H and N-H deformation	
3450–3360			O-H phenol deformation
2930–2880	C-H axial deformation		C-H axial deformation
1660			C=O carbonyl and keto-enol tautomerism
1655 (sh) *	Amide I		
1653 (sh) *		Amide I	
1640	O-H water bond		
1560	Amide II		
1558		Amide II	
1456		C-H pyrrolidine rings deformation	
1413	CH_2 axial deformation		
1385	CH_2 out-of-plane deformation		
1400-1350			C-O alcohol and phenol deformation
1240	O-H axial deformation		
1238		Amide III	
1190–960	C-O axial deformation		
1000	O-H and N-H deformation		C-H alkene deformation

* (sh) = stretching bands.

Other prominent bands are the ones in 1624 and 1524 cm^{-1}, which are related to the protonated amino groups of chitosan (NH_3^+), the ones in 1558 and 1238 cm^{-1}, which are characteristic of collagen amides II and III, respectively, and the band at 1000 cm^{-1}, which is related to the deformation of C-H bonds of the alkenes that are present in the structure of curcumin. The presence of these characteristic bands of the three components in the spectrum of Ch: Col: Cur20 (Figure 1d) shows the effectiveness of the incorporation of curcumin in the polymeric matrix, which will be attested by the rheological studies below.

3.2. Rheological Assays

3.2.1. Strain Sweep Measurements

The rheological study of chitosan and collagen solutions without curcumin and with curcumin at different concentrations started with the sweeping of their elastic and viscous moduli as a function of %strain; one of the main parameters for the characterization of the viscoelastic behavior of polymeric solutions is their linear viscoelastic region (LVR), that is,

the region in which the G′ and G″ moduli remain constant, regardless of the deformation to which the solution is subjected. The LVR is a direct indicator of the resistance of the solution to the applied deformation, and from its extension, it is possible to evaluate the structural strength of the polymeric network formed [26].

Figure 2a shows the graphs of G′ and G″ as a function of %strain; in all cases, the elastic modulus exceeded the viscous one (G′ > G″), which is characteristic of a solid-like behavior [26,27]. This behavior indicates that the solutions of chitosan and collagen had a gel-like structure and that their gel-like response was not affected by the incorporation of curcumin into the system. From the curves, it was possible to determine the parameters shown in Table 2: the first one, γ_{LVR}, is the critical deformation of the solutions, that is, the maximum deformation that can be applied before the LVR ends and the moduli decrease; the greater γ_{LVR} is, the more resistant to the applied deformation the solution will be. Likewise, the G'_{LVR} parameter is the value of the elastic modulus at the limit of the LVR, and it starts to decrease as soon as the LVR ends. For the solutions in this study, the incorporation of curcumin and the increase in its concentration in the chitosan and collagen matrix did not affect γ_{LVR} value, but interfered in the elastic behavior, leading to G'_{LVR} values up to 30 Pa lower in the Ch: Col: Cur10 solution when compared to the solution without curcumin. The increase in curcumin concentration, in turn, led to a gradual increase in the elastic moduli of the solutions, going from 43.96 to 57.46 Pa in Ch: Col: Cur50.

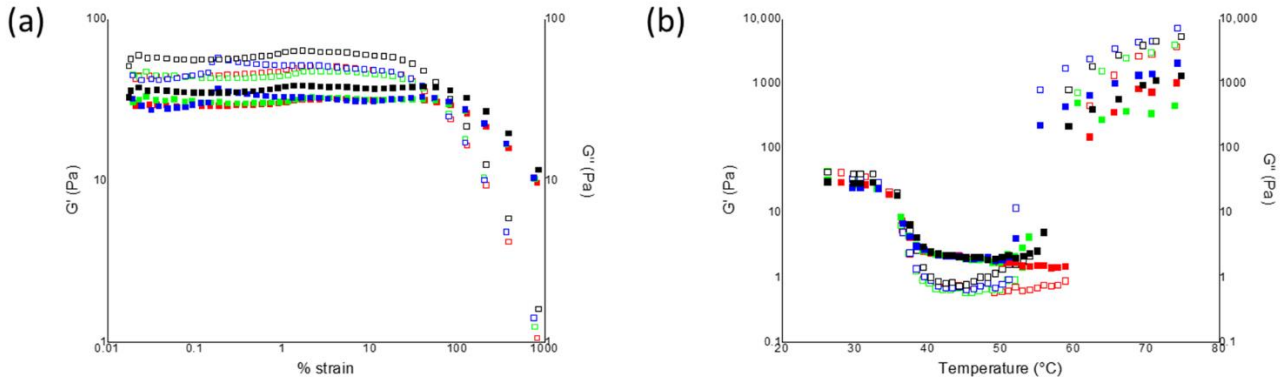


Figure 2. G′ and G″ moduli as a function of %strain (at 1 Hz and 25 °C) (**a**); G′ and G″ moduli as a function of temperature (25 to 75 °C, 5 °C min^{-1}, at 10% strain and 1 Hz) (**b**). G′ (empty symbols) and G″ (full symbols) for Ch: Col (▪), Ch: Col: Cur10 (▪), Ch: Col: Cur20 (▪), and Ch: Col: Cur50 (▪).

Table 2. Rheological parameters obtained from strain sweep, temperature sweep, and flow measurements: γ_{LVR}, critical deformation at the limit of the LVR; G'_{LVR}, elastic modulus value at the limit of the LVR; tanδ, G″/G′ ratio; G′–G″ difference at 1% strain; T and $G'_{crossover}$; η_0, viscosity at zero shear rate, obtained through the adjustment of the curves with the Cross model.

Parameter	Ch: Col	Ch: Col: Cur10	Ch: Col: Cur20	Ch: Col: Cur50
γ_{LVR} (%)	17.9	18.6	17.8	18.5
G'_{LVR} (Pa)	77.6	44.0	46.9	57.5
tanδ	0.5	0.7	0.7	0.6
G′-G″	35.7	13.7	18.5	24.0
$T_{crossover1}$ (°C)	33.8	32.9	34.7	35.3
$G'_{croosver1}$ (Pa)	14.5	15.5	13.8	13.2
$T_{crossover2}$ (°C)	59.8	53.9	51.6	55
$G'_{croosver2}$ (Pa)	7.4	4.1	2.7	3.5
η_0 (Pa s)	35.3	42.8	57.5	61.3

This effect of curcumin incorporation on the decrease in the elastic character of the solutions can also be observed in the tanδ parameter; as this parameter is the ratio between the viscous and elastic moduli, tanδ values < 1 indicate the predominance of G′ [28]. As

shown in Table 2, tanδ increased with the incorporation of curcumin into the polymeric matrix (which again points to a decrease in the elastic character of the solutions) and slightly decreased at higher curcumin concentrations.

Finally, the last parameter obtained from the strain sweep curves was the difference between the moduli at 1% strain (inside the LVR); G'–G" indicates whether the moduli are approaching or retreating from each other and reinforces the effect that the addition of the polyphenols brings to the system. As expected, the difference between the moduli decreased with the incorporation of curcumin, since the elastic modulus decreased. In general, this behavior can be explained by the greater number of interactions that were formed between the polyphenols of curcumin and the polymeric network of chitosan and collagen; phenolic compounds tend to accentuate the viscous moduli of polymeric solutions and, consequently, decrease their elastic character due to the new interactions formed [29]. However, the opposite effects were observed for the strain parameters in the solutions with higher concentrations of curcumin (i.e., a further increase in G'_{LVR} and in G'–G", as well as a further decrease in tanδ for Ch: Col: Cur20 and Ch: Col: Cur50), which may be an indication of a probable cross-linking of the polymeric network with higher concentrations of polyphenols [30].

3.2.2. Temperature Sweep Measurements

Figure 2b shows the curves of the G' and G" moduli as a function of temperature; in general, all solutions presented curves with similar profiles, starting with the predominance of G' at 25 °C. From 25 to 35 °C, a small plateau was observed in which both the elastic and viscous moduli remained constant, thus reflecting the stability of the polymeric matrix.

Right after this region, the first crossover between the moduli occurred, in which G' = G" and G" soon overcame the elastic modulus; this effect was associated with the thermal denaturation of collagen, whose triple helix collapsed into a random coil [31]. The temperature at which such an effect happens can also be called the collagen denaturation temperature (T_d) and is easily obtained at the point where G' = G" or where tanδ reaches its maximum [30]. In this study, the addition of curcumin to the polymeric matrix delayed the denaturation of collagen by about 1.5 °C (from 33.8 °C in Ch: Col to 35.3 °C in Ch: Col: Cur50) (Table 2), which is a new indicator of the possible cross-linking induced by this polyphenol.

From 35 to 50 °C, the elastic modulus of the solutions started to rise again, and in a more accentuated way than the predominant viscous modulus; the second crossover occurred above 50 °C for all solutions, which was an indicator of the gelling process in which G' became greater than G" again; this is also representative of a liquid–solid transition. This gelling point is associated with the elimination of energized water molecules at high temperatures, which rearranges the polymeric chains and leads to an increase in the elastic behavior of the solutions [27,29]. The addition of curcumin to the polymeric matrix led to a gelling point that was about 8 °C and 6 Pa lower for the Ch: Col: Cur20 solution when compared to Ch: Col, which was probably related to the initially smaller number of interactions between the polymers and water molecules due to the polyphenols' presence.

3.2.3. Flow Measurements

Figure 3 shows the viscosity curves as a function of the shear rate (s^{-1}) for the solutions; in the adopted shear rate range (from 1 to 1000 s^{-1}), all chitosan and collagen solutions—containing or not containing curcumin—presented a Newtonian behavior, that is, a decrease in viscosity with the application of shear. This behavior was associated with the ordering of polymeric chains, which were initially randomly distributed, when in the presence of shear [31].

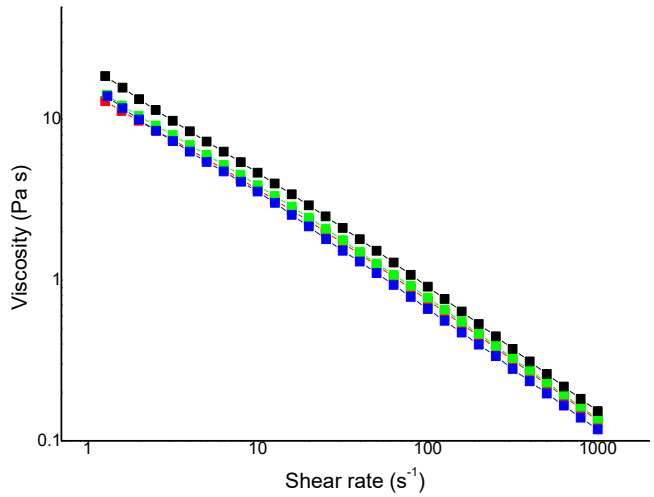


Figure 3. Viscosity (in Pa s) as a function of shear rate (s^{-1}) for Ch: Col (▪), Ch: Col: Cur10 (▪), Ch: Col: Cur20 (▪), and Ch: Col: Cur50 (▪).

From the adjustment of the curves with the Cross Equation (Equation (1), where η_0 is the zero-shear viscosity (Pa s), η_∞ is the viscosity limit at infinite shear (Pa s), γ is the shear rate (s^{-1}), k is the consistency index (s), and n is the rate index), it was possible to estimate the values of η_0, that is, the viscosity at zero shear (Table 2).

$$\frac{\eta - \eta_\infty}{\eta_0 - \eta_\infty} = \frac{1}{\left(1 + (k\gamma)^n\right)} \quad (1)$$

The incorporation of curcumin and the increase in its concentration promoted a linear effect of increasing the η_0 value of the solutions from 35.32 Pa s in Ch: Col to 61.27 Pa s in Ch: Col: Cur50. This effect of increasing the viscosity of polymeric solutions with the incorporation of polyphenols was already observed by Almeida et al. (2018) [32], who attributed it to the greater stiffness of a polymeric system containing curcumin.

Therefore, the results of the rheological assays (both oscillatory and steady shear) pointed to a proven interaction of curcumin with the polymeric network of chitosan and collagen, probably by cross-linking the amino groups of the polymeric matrix of collagen and chitosan with the OH and the keto groups of the curcumin structure. Moreover, a clear effect of curcumin concentration on the cross-linking of the polymeric system was observed. This cross-linking led to solutions with a more accentuated solid-like behavior, higher collagen denaturation temperatures, and higher viscosities, thus favoring their use as biomaterials for wound healing and tissue regeneration [30].

3.3. Thermogravimetric Analysis (TGA)

Once the rheological behavior of the chitosan and collagen solutions containing curcumin at different concentrations was elucidated and the effects that the polyphenol addition had on the polymeric matrix were evaluated, the solutions were frozen and lyophilized for the obtention of scaffolds. The thermal stability of the scaffolds was investigated for the scaffolds without curcumin (Ch: Col), as well as for the scaffolds with the lowest and highest amounts of polyphenol (that is, Ch: Col: Cur10 and Ch: Col: Cur50, respectively).

The thermogravimetric curves obtained, as well as their derivatives, are shown in Figure 4. All of the scaffolds with and without curcumin presented four stages of weight loss, whose percentages are displayed in Table 3. The first stage of weight loss, from 25 to 100 °C, represents the loss of absorbed water, ranging from 16.96 to 18.51%; next, the loss of structural water bound to the polymeric molecules in the scaffolds took place from 100 to 200 °C. The incorporation of curcumin led to percentages of bound water that were about 3.6% lower in relation to those of the Ch: Col scaffold (9.08%), which reinforces what the previous rheological results had pointed out: The presence of the curcuminoid decreased

the interaction sites in the polymeric network available for water contact, which also led to lower gelling temperatures.

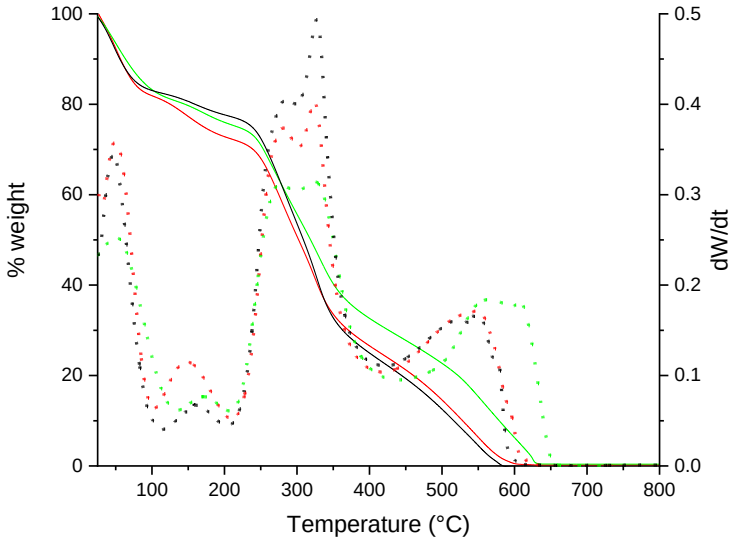


Figure 4. Thermogravimetric curves (solid lines) and their derivatives (dotted lines) for: (—) Ch: Col, (—) Ch: Col: Cur10, and (—) Ch: Col: Cur50.

Table 3. Weight loss and T_{onset} of the scaffolds determined through thermogravimetric analysis.

Scaffold	Weight Loss (%)				T_{onset} (°C)
	25–100 °C	100–200 °C	200–410 °C	410–750 °C	
Ch: Col	18.09	9.08	47.37	25.18	254.38
Ch: Col: Cur10	18.51	5.49	46.8	28.8	259.53
Ch: Col: Cur50	16.96	5.39	53.86	24.19	259.89

The third stage of weight loss of the thermogravimetric curves, from 200 to 410 °C, is related to the degradation of the collagen structure, and it presented the highest weight loss values, as well as the highest derivatives. From the peak of the derivatives in the third stage, it was possible to calculate T_{onset}, that is, the temperature at which the polymeric network started to degrade for each scaffold; again, the results of curcumin incorporation were promising, leading to T_{onset} values that were about 5 °C higher than in the case of the Ch: Col scaffold (Table 3). This result may be related to the cross-linking effect promoted by polyphenol, as mentioned in the rheological results. Finally, the last stage of weight loss, from 410 to 750 °C, refers to the decomposition and carbonization of the degradation products from the previous stage [11].

3.4. Scanning Electron Microscopy (SEM)

3.4.1. Surface and Cross-Sectional Surface Images

Figure 5 shows the appearances of the scaffolds obtained, as well as their surface and cross-sectional surface morphologies. The incorporation of curcumin into the polymeric matrix of chitosan and collagen led to changes in the coloration of the scaffolds, which changed from white (in the case of Ch: Col) to yellowish with the highest concentration of polyphenols (Ch: Col: Cur50). Regarding the surface morphology of the scaffolds (Figure 5a–c), all of them presented interconnected pores in the polymeric network, which is advantageous and desirable for the proposed application, since scaffolds must allow the transport of nutrients, absorb fluids and moisture, and allow cell migration and proliferation [33]. Moreover, there was a clear increase in the number of pores with the inclusion of curcumin compared to the compact matrix observed for Ch: Col. No agglomerates or precipitates of curcumin were observed along the surface of the scaffolds, which indicated

the homogeneity of the mixture and the complete miscibility of the polyphenol in the polymeric matrix.

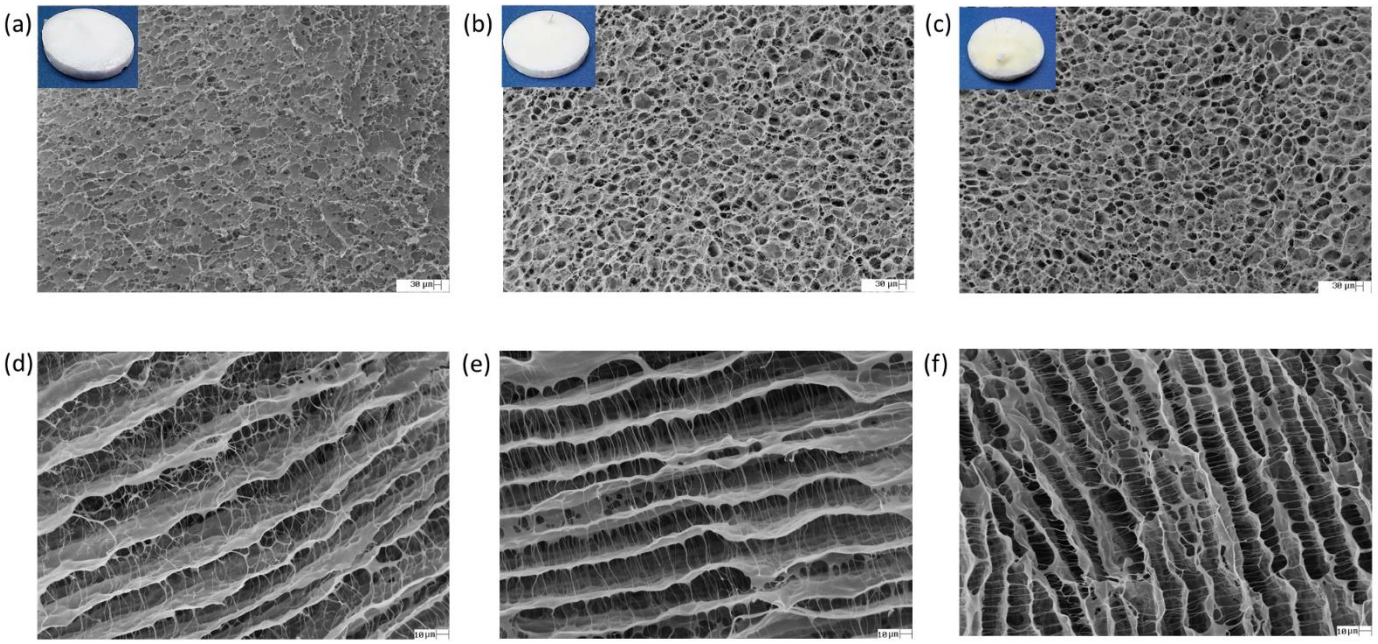


Figure 5. SEM images of the surface (200× magnification) and cross-sectional surface (1000× magnification), respectively, of Ch: Col (**a**,**d**), Ch: Col: Cur 10 (**b**,**e**), and Ch: Col: Cur 50 (**c**,**f**).

Regarding the cross-sectional surface micrographs of the scaffolds (Figure 5d–f), the polymeric fibers were channeled-distributed, and the addition of curcumin in its highest concentration led to a greater compaction of these channels, which was probably due to the cross-linking effect caused by the polyphenol. No visible agglomerates or precipitates of curcumin were observed in these cases either.

3.4.2. Pore and Channel Size

Once the surface and cross-sectional surface morphologies of the chitosan, collagen, and curcumin scaffolds were analyzed, the pore diameters of their surfaces were measured. The pore size of scaffolds intended to be applied as biomaterials in wound healings is one of the factors that most influences their performance and efficiency in the application; ideally, a scaffold must have pores with an adequate size to absorb moderate amounts of fluids (such as exudates that are released from the wound or injury) and to allow the maintenance of a moist environment in the wound bed at the same time [34].

Table 4 shows the average pore diameter values obtained for each sample. Although no statistically significant difference was observed between the samples, a clear tendency towards an increase in the pore diameter was noted for the scaffold with the highest concentration of curcumin, Ch: Col: Cur50, with an average diameter that was about 10 µm larger than the average diameter of the scaffolds without curcumin (Ch: Col) and the scaffolds with curcumin in a lower concentration (Ch: Col: Cur10). This effect of increasing the pore diameter of scaffolds based on biopolymers with the inclusion of bioactive compounds, such as phenols and polyphenols, was already observed by Bertolo et al. (2020) [35]; the inclusion of pomegranate peel extract (rich in phenolic compounds) in chitosan and gelatin scaffolds led to an increase in the diameter of the surface pores.

Table 4. Average pore size and channel size values for the scaffolds.

Scaffold	Pore Size (μm)	Channel Size (μm)
Ch: Col	35.15 ± 10.86 [a]	36.47 ± 7.30 [a]
Ch: Col: Cur10	35.14 ± 12.64 [a]	28.62 ± 2.36 [b]
Ch: Col: Cur50	45.31 ± 8.75 [a]	18.48 ± 2.30 [c]

[a, b, c] In the same column, values with different superscript letters indicate statistically different samples according to ANOVA and the Tukey test ($p \leq 0.05$).

Regarding the diameter of the channels observed in the cross-sectional images of the scaffolds, the effect of curcumin incorporation was opposite to the effect on the surface pores; Table 4 shows the average values obtained for the channels in each scaffold; in general, polyphenol promoted a greater compaction of the scaffolds' structure, leading to channels that were less spaced from each other. The difference in the size of the channels was statistically significant among the three scaffolds, and in the case of Ch: Col: Cur50, the channels (18.48 ± 2.30 μm) presented half the average diameter observed for Ch: Col (36.47 ± 7.30 μm).

Figure 6 shows the distribution of the pore diameter values measured for each of the scaffolds; the sample without curcumin (Figure 6a) presented a higher number of pores with diameters between 20 and 40 μm; with the addition of curcumin at its lowest concentration (Figure 6b), there was a shift of this higher number of pores to the region of 40–50 μm. When the amount of curcumin was increased (Figure 6c), the pore diameter distribution profile of the scaffolds changed completely, and a greater number of pores with diameters between 40 and 60 μm was observed.

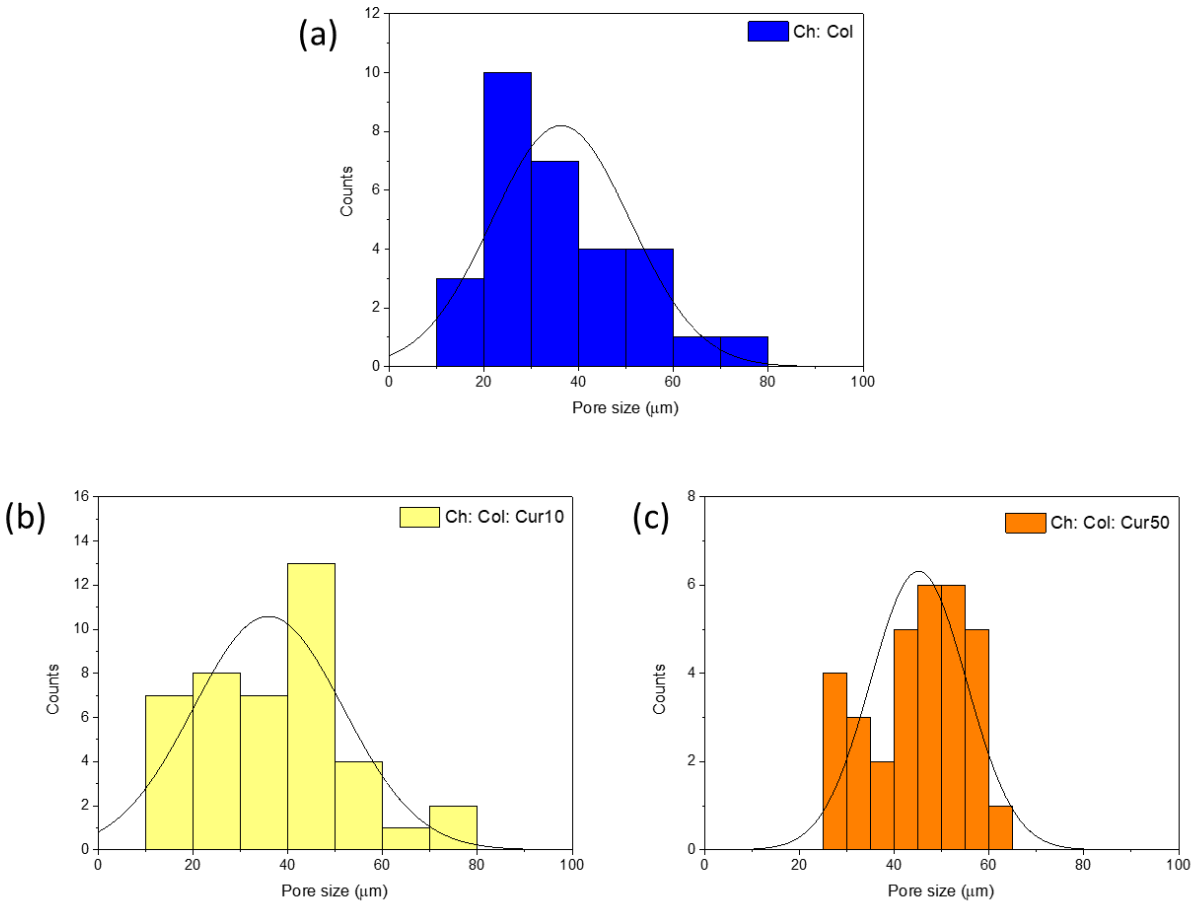


Figure 6. Pore size distribution for Ch: Col (**a**), Ch: Col: Cur10 (**b**), and Ch: Col: Cur50 (**c**).

Many studies in the literature have dealt with the optimal pore size for scaffolds that will be applied for tissue regeneration; the pore size is affected by many factors, including the choice of biopolymers and the presence of bioactive compounds (such as curcumin in this study). The type of tissue to be regenerated and that will be in contact with the scaffold also affects the optimal range desired. Ideally, pores with a range of 90 to 130 μm in diameter allow cell migration and proliferation, but in vitro results of cell growth in pores with diameters smaller than 100 μm have already been reported [36]. Furthermore, reports in the literature have already noted that microvascular epithelial cells generally require even smaller pores of about 40 μm for proliferation and differentiation [37]. In this case, the Ch: Col: Cur50 scaffold would be the most suitable for application in wound-healing applications, since it has a greater number of pores with diameters of around 40 μm and a structure with a greater number of channels that are interconnected with each other by smaller distances.

4. Conclusions

Curcumin was evaluated as a valuable bioactive compound in the development of chitosan- and collagen-based materials for wound-healing purposes due to its antioxidant, anti-inflammatory, and antiseptic properties. The effects of curcumin incorporation and concentration were evaluated for the rheological properties of Ch: Col solutions; the polyphenols decreased the elastic behavior of the polymers at low concentrations, but the opposite tendency of further increasing G' was observed with higher curcumin concentrations (20 and 50 mg). Likewise, both the elastic and viscous moduli were affected by temperature, and curcumin incorporation delayed the denaturation temperature of collagen (T_d) of the scaffolds by about 1.5 °C. The TGA results also showed promising effects of curcumin on delaying the temperature at which scaffolds start to degrade by about 5 °C. The cross-linking brought by the polyphenols was also reflected in the greater viscosity and stiffness of the solutions, as well as in the greater compaction of the polymer channels in the cross-sectional surface images obtained with SEM. The diameters of the surface pores increased according to the increase in curcumin concentration, ranging mainly from 40 to 60 μm for Ch: Col: Cur50, the most suitable scaffold for the continuation of the biological and in vitro studies that are necessary for the proposed application.

Author Contributions: Conceptualization, E.P.M., V.C.A.M. and A.M.G.P.; methodology, E.P.M. and V.C.A.M.; writing—original draft preparation, E.P.M. and M.R.V.B.; writing—review and editing, V.C.A.M., S.B.J. and A.M.G.P.; supervision, A.M.G.P.; project administration, A.M.G.P. All authors have read and agreed to the published version of the manuscript.

Funding: This study was supported by the Coordenação de Aperfeiçoamento de Pessoal de Nível Superior—Brasil (CAPES)—Finance Code 001.

Institutional Review Board Statement: Not applicable.

Informed Consent Statement: Not applicable.

Acknowledgments: The authors would like to thank the Center of Analytical Chemical Analysis of IQSC/USP for the infrastructure that was made available for the FTIR and SEM analyses. We also thank Eder Tadeu Gomes Cavalheiro and Ana Paula Garcia Ferreira (IQSC/USP) for the access to the TGA-Q50 instrument. Finally, we thank the Fundação de Amparo à Pesquisa do Estado de São Paulo (FAPESP) for the grant to M.R.V.B. (2019/18748-8).

Conflicts of Interest: The authors declare no conflict of interest.

References

1. Pattanayak, S.P.; Sunita, P. Wound healing, anti-microbial and antioxidant potential of *Dendrophthoe falcata* (L.f) Ettingsh. *J. Ethnopharmacol.* **2008**, *120*, 241–247. [CrossRef] [PubMed]
2. Yu, R.; Zhang, H.; Guo, B. Conductive biomaterials as bioactive wound dressing for wound healing and skin tissue engineering. *Nano-Micro Lett.* **2022**, *14*, 751. [CrossRef] [PubMed]

3. Wu, M.; Lu, Z.; Wu, K.; Nam, C.; Zhang, L.; Guo, J. Recent advances in the development of nitric oxide-releasing biomaterials and their application potentials in chronic wound healing. *J. Mater. Chem. B* **2021**, *9*, 7063–7075. [CrossRef] [PubMed]
4. Dharunya, G.; Duraipandy, N.; Lakra, R.; Korapatti, P.S.; Jayavel, R.; Kiran, M.S. Curcumin cross-linked collagen aerogels with controlled anti-proteolytic and pro-angiogenic efficacy. *Biomed. Mater.* **2016**, *11*, 045011. [CrossRef]
5. Cheng, A.; Schwartz, Z.; Kahn, A.; Li, X.; Shao, Z.; Sun, M.; Ao, Y.; Boyan, B.D.; Chen, H. Advances in porous scaffold design for bone and cartilage tissue engineering and regeneration. *Tissue Eng. Part B Rev.* **2019**, *25*, 14–29. [CrossRef]
6. Amiri, N.; Ajami, S.; Shahroodi, A.; Jannatabadi, N.; Amiri Darban, S.; Fazly Bazzaz, B.S.; Pishavar, E.; Kalalinia, F.; Movaffagh, J. Teicoplanin-loaded chitosan-PEO nanofibers for local antibiotic delivery and wound healing. *Int. J. Biol. Macromol.* **2020**, *162*, 645. [CrossRef]
7. Bayat, S.; Amiri, N.; Pishavar, E.; Kalalinia, F.; Movaffagh, J.; Hashemi, M. Bromelain-loaded chitosan nanofibers prepared by electrospinning method for burn wound healing in animal models. *Life Sci.* **2019**, *229*, 57–66. [CrossRef]
8. Chattopadhyay, S.; Raines, R.T. Collagen-based biomaterials for wound healing. *Biopolymers* **2014**, *101*, 821–833. [CrossRef]
9. Chen, Y.; Lee, K.; Yang, Y.; Kawazoe, N.; Chen, G. PLGAcollagen-ECM hybrid meshes mimicking stepwise osteogenesis and their influence on the osteogenic differentiation of hMSCs. *Biofabrication* **2020**, *12*, 025027. [CrossRef]
10. Elhendawi, H.; Felfel, R.M.; El-Hady, A.; Bothaina, M.; Reicha, F.M. Effect of synthesis temperature on the crystallization and growth of in situ prepared nanohydroxyapatite in chitosan matrix. *Biomaterials* **2014**, *2014*, 897468. [CrossRef]
11. Bertolo, M.R.V.; Martins, V.C.A.; de Guzzi Plepis, A.M. Effects of calcium phosphates incorporation on structural, thermal and drug-delivery properties of collagen:chitosan scaffolds. *Int. J. Adv. Med. Biotechnol.-IJAMB* **2020**, *2*, 25–35. [CrossRef]
12. Sultankulov, B.; Berillo, D.; Sultankulova, K.; Tokay, T.; Saparov, A. Progress in the development of chitosan-based biomaterials for tissue engineering and regenerative medicine. *Biomolecules* **2019**, *9*, 470. [CrossRef] [PubMed]
13. Lin, K.; Zhang, D.; Macedo, M.H.; Cui, W.; Sarmento, B.; Shen, G. Advanced collagen-based biomaterials for regenerative biomedicine. *Adv. Funct. Mater.* **2019**, *29*, 1804943. [CrossRef]
14. Hatcher, H.; Planalp, R.; Cho, J.; Torti, F.M.; Torti, S.V. Curcumin: From ancient medicine to current clinical trials. *Cell. Mol. Life Sci.* **2008**, *65*, 1631–1652. [CrossRef]
15. Abbas, M.; Hussain, T.; Arshad, M.; Ansari, A.R.; Irshad, A.; Nisar, J.; Hussain, F.; Masood, N.; Nazir, A.; Iqbal, M. Wound healing potential of curcumin cross-linked chitosan/polyvinyl alcohol. *Int. J. Biol. Macromol.* **2019**, *140*, 871–876. [CrossRef] [PubMed]
16. Fathima, N.N.; Devi, R.S.; Rekha, K.B.; Dhathathreyan, A. Collagen–curcumin interaction—A physico-chemical study. *J. Chem. Sci.* **2009**, *121*, 509–514. [CrossRef]
17. Rezaei, M.; Oryan, S.; Nourani, M.R.; Mofid, M.; Mozafari, M. Curcumin nanoparticle-incorporated collagen/chitosan scaffolds for enhanced wound healing. *Bioinspired Biomim. Nanobiomater.* **2018**, *7*, 159–166. [CrossRef]
18. Rezaei, M.; Oryan, S.; Javeri, A. Curcumin nanoparticles incorporated collagen-chitosan scaffold promotes cutaneous wound healing through regulation of TGF-β1/Smad7 gene expression. *Mater. Sci. Eng. C* **2019**, *98*, 347–357. [CrossRef]
19. Jirofti, N.; Golandi, M.; Movaffagh, J.; Ahmadi, F.S.; Kalalinia, F. Improvement of the wound-healing process by curcumin-loaded chitosan/collagen blend electrospun nanofibers: In vitro and in vivo studies. *ACS Biomater. Sci. Eng.* **2021**, *7*, 3886–3897. [CrossRef]
20. Horn, M.M.; Martins, V.C.A.; Plepis, A.M.G. Interaction of anionic collagen with chitosan: Effect on thermal and morphological characteristics. *Carbohydr. Polym.* **2009**, *77*, 239–243. [CrossRef]
21. Lavertu, M.; Xia, Z.; Serreqi, A.N.; Berrada, M.; Rodrigues, A.; Wang, D.; Buschmann, M.D.; Gupta, A. A validated ^{1}H NMR method for the determination of the degree of deacetylation of chitosan. *J. Pharm. Biomed. Anal.* **2003**, *32*, 1149–1158. [CrossRef]
22. Rinaudo, M. Chitin and chitosan: Properties and applications. *Prog. Polym. Sci.* **2006**, *31*, 603–632. [CrossRef]
23. Cai, L.; Shi, H.; Cao, A.; Jia, J. Characterization of gelatin/chitosan ploymer films integrated with docosahexaenoic acids fabricated by different methods. *Sci. Rep.* **2019**, *9*, 8375. [CrossRef] [PubMed]
24. Batista, T.M.; Martins, V.C.A.; Plepis, A.M.G. Thermal behavior of in vitro mineralized anionic collagen matrices. *J. Therm. Anal. Calorim.* **2009**, *95*, 945–949. [CrossRef]
25. Chen, X.; Zou, L.-Q.; Niu, J.; Liu, W.; Peng, S.-F.; Liu, C.-M. The stability, sustained release and cellular antioxidant activity of curcumin nanoliposomes. *Molecules* **2015**, *20*, 14293–14311. [CrossRef]
26. Steffe, J.F. *Rheological Methods in Food Process Engineering*; Freeman Press: East Lansing, MI, USA, 1996.
27. Silva-Weiss, A.; Bifani, V.; Ihl, M.; Sobral, P.; Gómez-Guillén, M.C. Structural properties of films and rheology of film-forming solutions based on chitosan and chitosan-starch blend enriched with murta leaf extract. *Food Hydrocoll.* **2013**, *31*, 458–466. [CrossRef]
28. Razmkhah, S.; Mohammad, S.; Razavi, A. Dilute solution, flow behavior, thixotropy and viscoelastic characterization of cress seed (*Lepidium sativum*) gum fractions. *Food Hydrocoll.* **2017**, *63*, 404–413. [CrossRef]
29. Romanelli Vicente Bertolo, M.; Leme, R.; da Conceição Amaro Martins, V.; de Guzzi Plepis, A.M.; Bogusz Junior, S. Rheological characterization of the influence of pomegranate peel extract addition and concentration in chitosan and gelatin coatings. *Polysaccharides* **2021**, *2*, 648–660. [CrossRef]
30. Kaczmarek, B.; Mazur, O. Collagen-based materials modified by phenolic acids—A review. *Materials* **2020**, *13*, 3641. [CrossRef]
31. Mandala, I.; Savvas, T.; Kostaropoulos, A. Xanthan and locust bean gum influence on the rheology and structure of a white model-sauce. *J. Food Eng.* **2004**, *64*, 335–342. [CrossRef]

32. Almeida, C.M.R.; Magalhães, J.M.C.S.; Souza, H.K.S.; Gonçalves, M.P. The role of choline chloride-based deep eutectic solvent and curcumin on chitosan films properties. *Food Hydrocoll.* **2018**, *81*, 456–466. [CrossRef]
33. Leong, K.F.; Chua, C.K.; Sudarmadji, N.; Yeong, W.Y. Engineering functionally graded tissue engineering scaffolds. *J. Mech. Behav. Biomed. Mater.* **2008**, *1*, 140–152. [CrossRef] [PubMed]
34. Negut, I.; Dorcioman, G.; Grumezescu, V. Scaffolds for wound healing applications. *Polymers* **2020**, *12*, 2010. [CrossRef] [PubMed]
35. Bertolo, M.R.V.; Martins, V.C.A.; Horn, M.M.; Brenelli, L.B.B.; Plepis, A.M.G. Rheological and antioxidant properties of chitosan/gelatin-based materials functionalized by pomegranate peel extract. *Carbohydr. Polym.* **2020**, *228*, 115386. [CrossRef]
36. Chong, E.J.; Phan, T.T.; Lim, I.J.; Zhang, Y.Z.; Bay, B.H.; Ramakrishna, S.; Lim, C.T. Evaluation of electrospun PCL/gelatin nanofibrous scaffold for wound healing and layered dermal reconstitution. *Acta Biomater.* **2007**, *3*, 321–330. [CrossRef]
37. Bruzauskaite, I.; Bironaite, D.; Bagdonas, E.; Bernotiene, E. Scaffolds and cells for tissue regeneration: Different scaffold pore sizes—different cell effects. *Cytotechnology* **2016**, *68*, 355–369. [CrossRef]